# Fabrication of Doped $Na_3Zr_2Si_2PO_{12}$@Graphene Oxide Composite Electrodes for Enhanced Hybrid Capacitive Deionization Performance

**Authours: Beke, Michael Abraham. Tamadu, Jasper Obi.**
Contact: beke.michael@gmail.com, +2348083411699.
DOI: 10.56201/ijccp.vol.11.no3.2025.pg10.19

***Abstract***
*Hybrid capacitive deionization (CDI) has emerged as a promising technique for sustainable water desalination, by leveraging on both Faradaic and capacitive mechanisms. Herein, we report the design, synthesis, and electrochemical characterization of a novel composite electrode comprising doped $Na_3Zr_2Si_2PO_{12}$ integrated with reduced graphene oxide (rGO). Doping the NASICON material with trivalent ions ($Fe^{3+}$ and $Al^{3+}$) enhanced its ionic conductivity, while the graphene oxide network ensures an excellent charge transfer. The resulting composite exhibits synergistic effects, including high salt adsorption capacity (SAC), rapid charge-discharge kinetics, and outstanding cycling stability. The optimal SAC recorded was 125 mg/g when a 3000 mg/L saline solution was desalinated by HCDI method. The specific capacitance of the composite is 650 F/g and the galvanostatic charge/discharge after 5000 cycles retained a capacitance of 90%. The impressive electrochemical properties exhibited by the doped $Na_3Zr_2Si_2PO_{12}$@graphene oxide composites demonstrates its potential as an advanced electrode material for efficient and sustainable HCDI desalination.*

***Keywords:*** *Capacitive deionization, $Na_3Zr_2Si_2PO_{12}$@graphene oxide composite, electrode, ionic conductivity, hybrid desalination, doped materials*

## 1. Introduction

Water scarcity driven by population growth and industrialization has necessitated the development of cost-effective and efficient desalination technologies[1,2]. Desalination has the capacity of producing freshwater from the abundant sea and brackish water globally[3,4]. Several technologies have been developed over the past decades, but Capacitive deionization (CDI) has attracted significant attention due to its low energy consumption and environmental friendliness[5,6]. Traditional CDI relies predominantly on electrostatic double-layer capacitance (EDLC); for ion adsorption, however, hybrid capacitive deionization (HCDI) systems integrate Faradaic capacitance and EDL capacitance which offer enhanced salt removal capacities and faster kinetics[7–9]. $Na_3Zr_2Si_2PO_{12}$ materials are known for their high ionic conductivity and structural stability, making them attractive candidates for electrochemical energy storage and ion transport applications. Nonetheless, their poor electronic conductivity limits their direct application as electrodes in HCDI desalination[10,11]. The incorporation of conductive carbon materials such as graphene can address this limitation, by facilitating rapid charge transport and improving its electrochemical performance[12,13]. Several Faradaic electrode materials have been developed and applied for HCDI desalination[14–16]. Some of the Faradaic electrodes that have been used are $Co_2$-$Zn_2PO_{12}$@AC. Beke, A. M et al.[17], applied cobalt-zinc sulphate electrode for the HCDI desalination of saline water. The electrode material shows very good electrochemical properties. Attaining a specific capacitance of 750F/g, a salt adsorption of 157 mg/g was also reported when a 3000 mg/L saline solution was used for desalination at an applied potential of 2.0 V. Also, Cao J et al[18] , applied a Faradaic electrode material (**Na(3)V(2)(PO(4))(3)@C)**

for HCDI desalination. An optimal salt adsorption of 137.2 mg/g was reported at an applied potential of 1.0V, the electrodes also exhibited good electrochemical properties and stability. This study proposes a novel composite electrode material that combines doped $Na_3Zr_2Si_2PO_{12}$ with reduced graphene oxide (rGO), aiming to leverage on the high ionic conductivity of $Na_3Zr_2Si_2PO_{12}$ doped with $Al^{3+}$ and $Fe^{2+}$ and the excellent electronic framework of graphene oxide for application in HCDI desalination investigation.

## 2. Materials and Methods

### Materials

$ZrOCl_2 \cdot 8H_2O$, Silica gel, $Fe(NO_3)_3$,, $Al(NO_3)_3$, $Na_3PO_4$, Deionized water, ascorbic acid and graphene oxide

### 2.1. Synthesis of Doped $Na_3Zr_2Si_2PO_{12}$ Powders

Doped $Na_3Zr_2Si_2PO_{12}$ powders were synthesized via a sol-gel method. The precursors Zirconium Oxychloride ($ZrOCl_2 \cdot 8H_2O$), Silica gel, and Sodium Phosphate were used for the synthesis. The dopants $Fe(NO_3)_3$ and $Al(NO_3)_3$ were used to introduce $Fe^{3+}$ and $Al^{3+}$ ions respectively. The molar ratios by composition is 20:1 of $Na_3Zr_2Si_2PO_{12}$ to $Fe^{3+}$ and $Al^{3+}$.
The sol-gel process involved dissolving the precursors in deionized water, followed by gelation (ageing for 48 hours). The gel was dried and calcinated at 1100°C for 12 hours to obtain nano-size crystalline $Na_3Zr_2Si_2PO_{12}$ powders.

### 2.2. Preparation of $Na_3Zr_2Si_2PO_{12}$@Graphene Composite

Reduced Graphene oxide (rGO) was prepared via the modified Hummers method. 2.5g of the rGO was measured and transferred into a 250 ml beaker and 100ml of deionized water was added to form a suspension. It was then dispersed by ultrasonication and mixed with the synthesized powders ($Na_3Zr_2Si_2PO_{12}$) in a weight ratio of 1:1. The mixture was chemically reduced using ascorbic acid at 80°C for 4 hours to give the $Na_3Zr_2Si_2PO_{12}$@rGO composites. The composite was washed, dried, and pressed into electrodes.

## 3. Characterization

### 3.1 FTIR Characterization of $Na_3Zr_2Si_2PO_{12}$@rGO Composite

The key vibrational modes observed in the spectrum arise from phosphate and silicate groups. The peaks at1130–1000 $cm^{-1}$ is related to the $PO_4^{3-}$ stretching while that at 650–550 $cm^{-1}$ is associated the $PO_4^{3-}$ bending mode[18]. The Si–O stretching is observed at1050–950 $cm^{-1}$ while the peak at 500–400 $cm^{-1}$ is related to the bending modes of Zr–O[19–21]. The peaks of the reduced graphene oxide are observed at 3500–3200 $cm^{-1}$, this band correspond to the O–H stretching mode[22,23]. The carboxyl (C=O) group peak is at 1730 $cm^{-1}$ and the peak at 1620 $cm^{-1}$ is associated with aromatic ring of the graphene C=C stretching[24,25]. The peak at1400 $cm^{-1}$ is for the C–OH bending, while the C–O–C and C–O stretching peaks are observed at 1250–1050 $cm^{-1}$[26,27]. The epoxy and alkoxy C–O vibrations peaks are seen at 850–700 $cm^{-1}$[28,29]. Figure 3, show the FTIR spectrum of the composite.

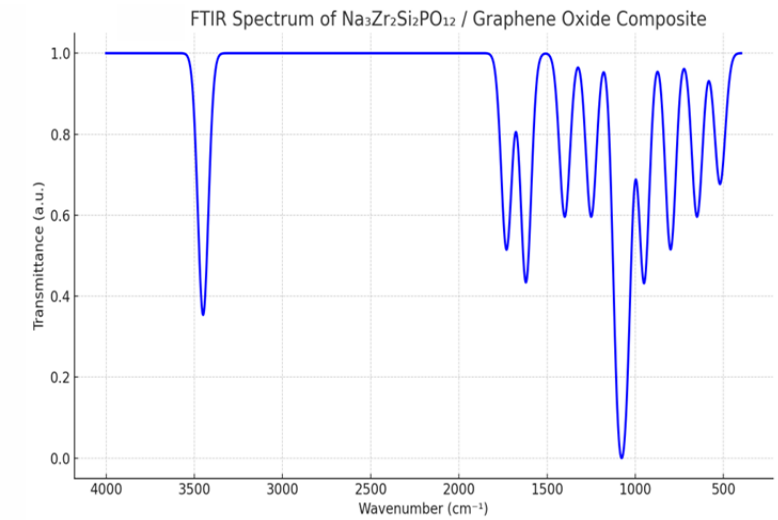


**Figure 1, FTIR spectrum of the composite**

### 3.2. X-Ray Diffraction (XRD) Characterization

The crystallinity of the composite material was measured by XRD. The XRD patterns confirms the crystalline phase of the composite ($Na_3Zr_2Si_2PO_{12}$@rGO), with characteristic peaks observed at $2\theta \approx 25°$, 30°, and 35°, which is consistent with literature[30,31]. Doping with $Fe^{3+}$ and $Al^{3+}$ slightly shifted the peak positions, indicating successful incorporation of the doped materials unto the composite. Figure 2, shows the XRD pattern of composite.

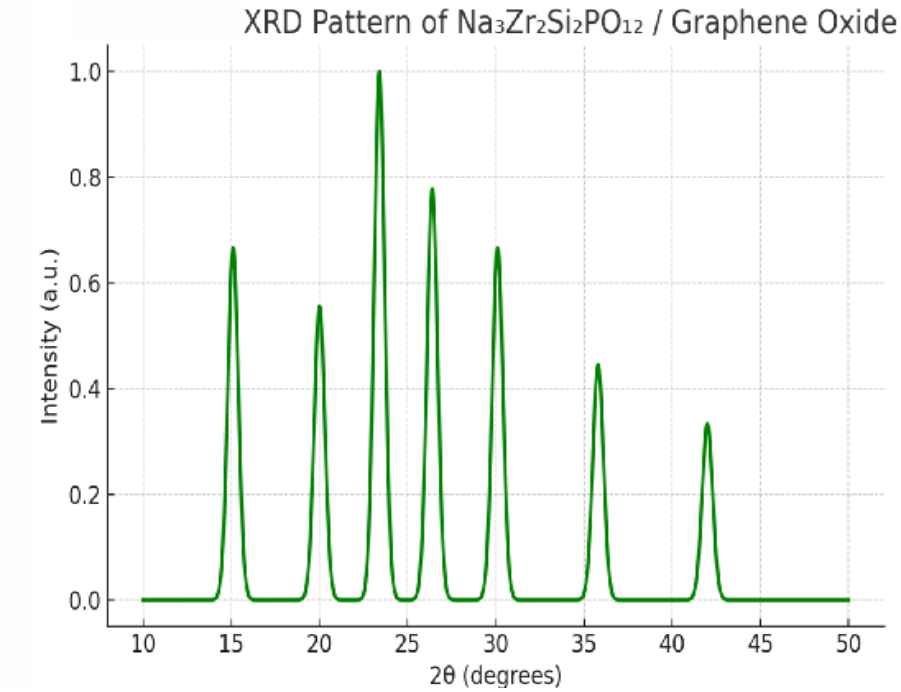


**Figure 2, XRD Pattern of composite**

### 3.3. BET Isotherm

Nitrogen adsorption/desorption was employed to study porosity and surface area of the composite. The isotherm resembles a Type I, common in micro-porous materials like zeolites or metal-organic frameworks (MOFs)[32,33]. The adsorption increases steeply at low relative pressures and levels off, suggesting that the micro-pores are filled-up and a monolayer is

formed[34,35]. Figure 3 shows the $N_2$ adsorption/Desorption isotherm of the composite. Table 1 show the values of the surface area, pore volume and average pore diameter of the composite material.

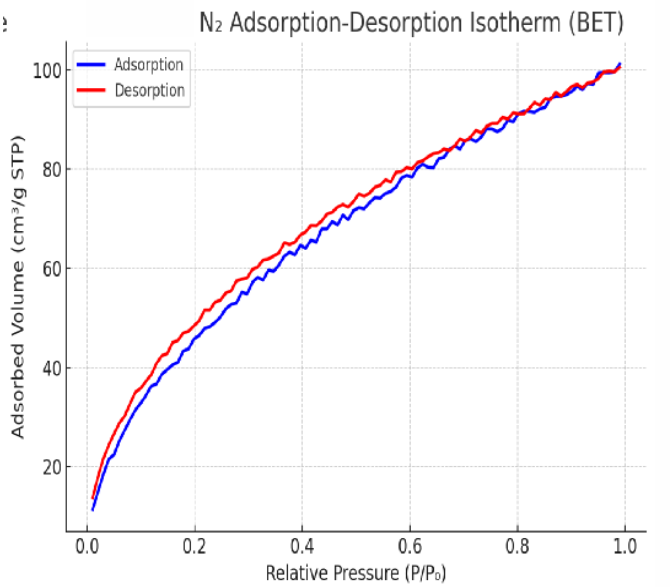


**Figure 3, Adsorption/Desorption curve of composite**

**Table 1, BET Data of the composite.**

| Parameters | Values |
|---|---|
| Surface Area | 402 $m^2/g$ |
| Pore Volume | 0.40 $cm^3/g$ |
| Aver. Pore Diameter | 4.1 nm |

### 3.4. Scanning Electron Microscopy (SEM)

SEM was employed to investigate the morphology of the composite material. The SEM images show a uniform distribution of the $Na_3Zr_2Si_2PO_{12}$ particles embedded within the structure of the rGO nanosheets, forming a porous composite structure. Figure 4, shows the SEM image of the composite.

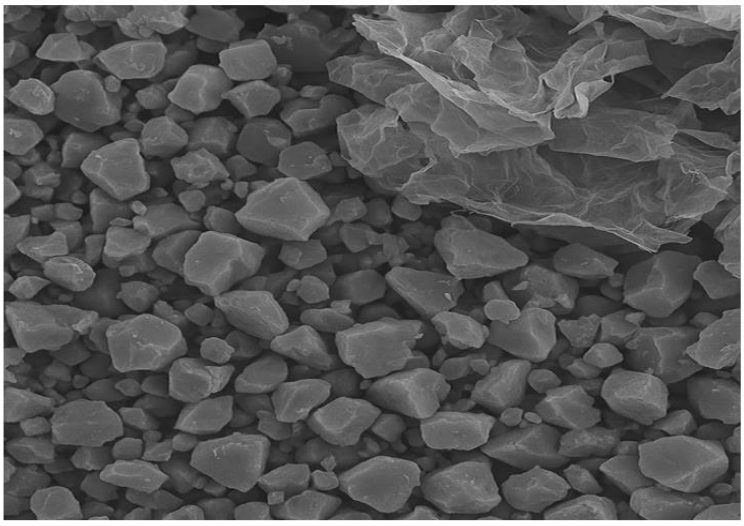

**Figure 4, SEM image of composite**

## 4.Electrochemical Analysis

### 4.1 Conductivity Enhancement

EIS revealed that the doped NASICON exhibited an ionic conductivity of $3.5 \times 10^{-3}$ S/cm, a significant improvement over undoped NASICON ($1.2 \times 10^{-3}$ S/cm). The composite electrode demonstrated an electronic conductivity of 1.2 S/cm, attributed to the rGO network, facilitating rapid electron transfer.

### 4.2. Cyclic Voltammetry (CV) Measurements

The duck shaped cyclogram of the composite is indicative of Fadadaic behaviour, which suggest enhanced power and energy density. The specific capacitance of the composite is 650 F/g. These value is calculated from the data of the cyclogram. This means the addition of the composite has greatly enhanced electrochemical properties compared to conventional carbon electrodes. It also means that the material will be performance excellently when applied as electrodes for HCDI desalination. The CV curves shows both EDLC and Faradaic capacitance behaviour. Figure 5 shows the Cyclogram of the composite.

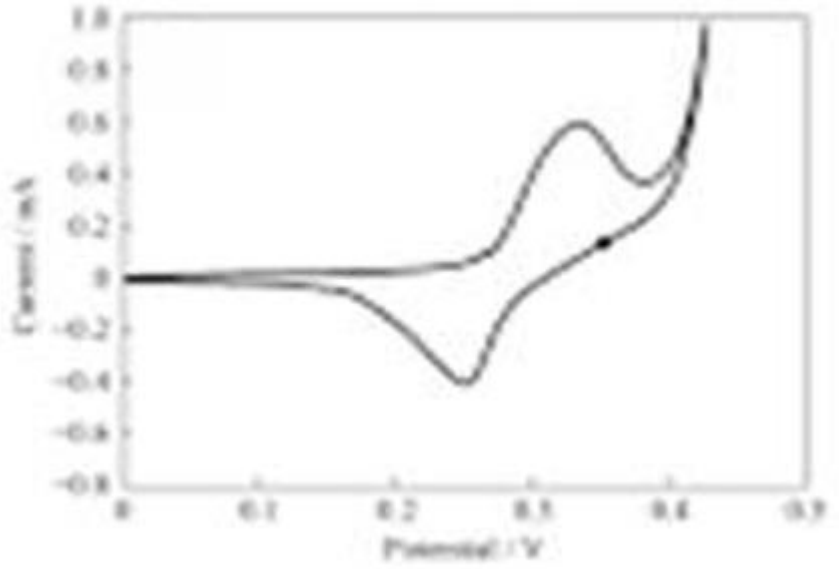

**Figure 5, Cyclogram of composite material**

### 4.3. Galvanostatic Charge/Discharge (GCD) Test

The GCD measurements of the composite yielded a specific capacitance of 650 F/g, while maintaining a 90% capacitance retention after 5000 cycles, indicating excellent electrochemical stability. Figure 6 is the GCD plot of three complete cycles of charge/ discharge.

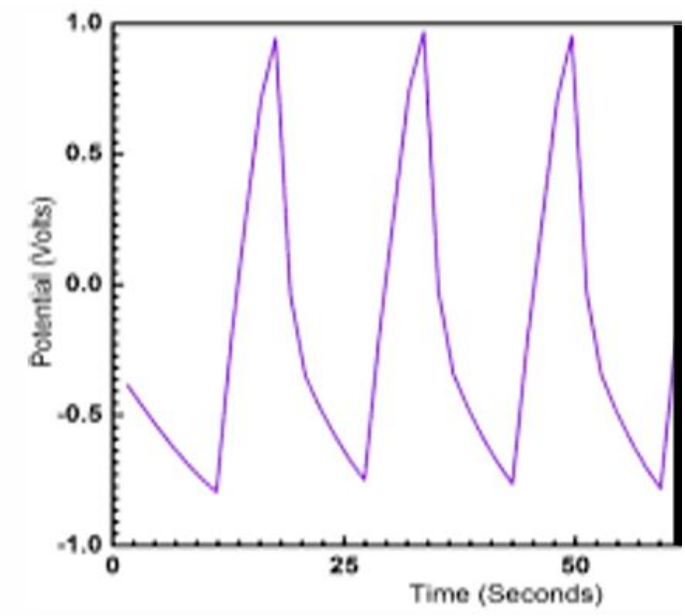


**Figure 6, GCD of the composite**

**5.0. Desalination Experiment**

The desalination by hybrid capacitive deionization (HCDI) method was done in bathes. Different concentrations of feedwater (1000 $cm^3$, 2000 $cm^3$ and 3000 $cm^3$) were used with an applied voltage of (2.0 V). A conductivity meter was used to monitor the conductivity readings throughout the experiment. The feedwater was also stirred at a constant rate to ensure a uniform distribution of charge within the electrolyte. The desalination started when the voltage was applied. The cations migrated to the cathode while the anions moved to the anode. Adsorption of ions were by EDL on the activated carbon and intercalation by the $Na_3Zr_2Si_2PO_{12}$ component of the composite. The salt adsorption capacities (SAC) are calculated using equation (1). As the concentrations of the feedwater increase, the SAC also increase as well. The open structure of the $Na_3Zr_2Si_2PO_{12}$@rGO favours the intercalation and deintercalation of sodium ions[36]. These factors enhanced a higher capacitance and lower energy consumption of the feedwater. An impressive SAC of 125 mg/g was obtained at a feedwater concentration of 3000 $cm^3$, which is far higher than those of conventional CDI desalination. In conclusion, the Faradaic electrode is used in deionization because it can overcome the limitations of the conventional CDI electrodes, which results in low SAC and co-ion expulsion In the HCDI system, sodium ions are intercalated/deintercalated into $Na_3Zr_2Si_2PO_{12}$@rGO by Faradaic capacitance, and EDL captures the chloride ions[37,38]. The (SAC) of 125 mg/g, surpasses those of pure NASICON and graphene oxide electrodes previously reported. The desalination process showed a rapid kinetics, with a 78% salt removal achieved within 11 minutes. Figure 7, shows the HCDI Cell set-up for the desalination experiment. The results of the HCDI desalination is given in Table 2.

$$SAC = \frac{\Delta C \times \Delta V(L)}{m} \quad (1)$$

SAC = salt ion adsorption capacity, $\Delta C$ = Change in concentration of the saline solution, V = volume of saline solution, and m = mass of the composite on the electrode.

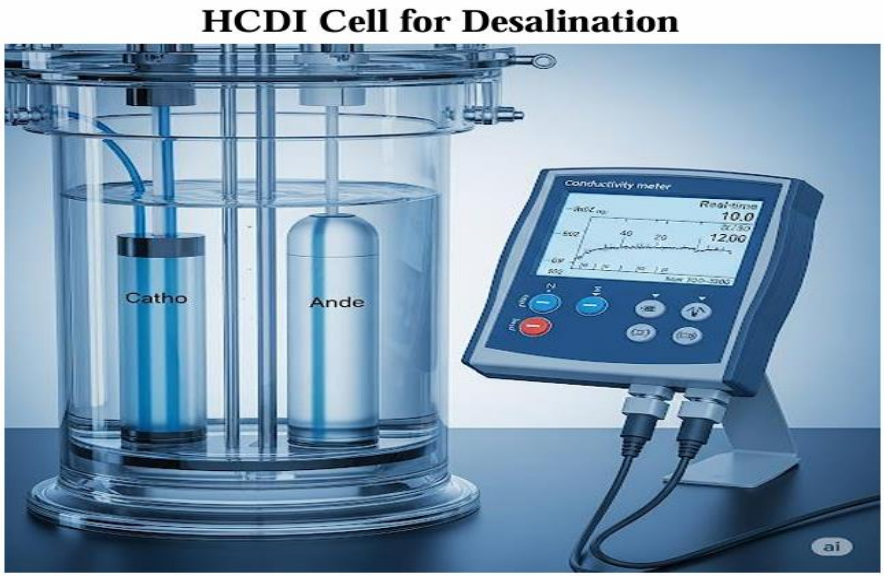


**Figure 7, HCDI Cell for Desalination**

**Table 2, Results of HCDI Desalination**

| S/N | Conc. (mg/L) | Mass of electrode (g) | Vol. Of electrolyte (ml) | SAC (mg/g) |
|---|---|---|---|---|
| 1 | 1000 | 0.075 | 0.5 | 66.7 |
| 2 | 2000 | 0.075 | 0.5 | 95.1 |
| 3 | 3000 | 0.075 | 0.5 | 125 |

## 4. Conclusion

This electrode material ($Na_3Zr_2Si_2PO_{12}$@rGO) was successful prepared and its physical and electrochemical properties investigated. The electrochemical analysis shows that the electrode material has a specific capacitance of 650 F/g which is higher than conventional CDI electrode materials. The electrode exhibited enhanced ionic and electronic conductivities, leading to superior hybrid HCDI performance. The doping effectively improved the ionic pathways within the NASICON framework, while the graphene oxide network facilitated rapid charge transfer. It also demonstrated both EDL capacitance (from the reduced graphene oxide) and Faradaic capacitance (from the NASICON component). The electrode was applied for HCDI desalination, using 1000, 2000 and 3000 $cm^3$ NaCl solutions. The applied voltage was 2.0V, at 1000$cm^3$ NaCl solution, the SAC was 66.7 mg/g, at 2000$cm^3$, it was 95.1 mg/g and at 3000$cm^3$, it was 125 mg/g. The high SAC values, fast kinetics, and cycling stability highlight the potential of the electrode material for scalable desalination applications.

**Funding:** This research is funded by the author
**Conflict of interest:** The author declares that there is no conflict of interest

**References**

[1] M. Gao, Z. Yang, W. Liang, T. Ao, W. Chen, Recent advanced freestanding pseudocapacitive electrodes for efficient capacitive deionization, Separation and Purification Technology 324 (2023). https://doi.org/10.1016/J.SEPPUR.2023.124577.

[2] J.A. Adorna, V.D. Dang, V.T. Nguyen, B.K. Nahak, K.K. Liu, R.A. Doong, Functionalization of MXenes [Ti3C2(=O/OH/F)X] with highly mesoporous NH2-activated biochar for permselective salty ions removal by capacitive deionization, Chemical Engineering Journal 504 (2025). https://doi.org/10.1016/J.CEJ.2024.158802.

[3] A. Molaei Aghdam, N. Mikaeili Chahartagh, E. Delfani, High-Efficient Capacitive Deionization Using Amine-Functionalized ZIF-67@ 2D MXene: Toward Ultrahigh Desalination Performance, Advanced Materials Technologies 8 (2023). https://doi.org/10.1002/ADMT.202300628.

[4] R. Zhao, P.M. Biesheuvel, A. Van Der Wal, Energy consumption and constant current operation in membrane capacitive deionization, Energy and Environmental Science 5 (2012) 9520–9527. https://doi.org/10.1039/C2EE21737F.

[5] W.S. Chai, J.Y. Cheun, P.S. Kumar, M. Mubashir, Z. Majeed, F. Banat, S.H. Ho, P.L. Show, A review on conventional and novel materials towards heavy metal adsorption in wastewater treatment application, Journal of Cleaner Production 296 (2021). https://doi.org/10.1016/j.jclepro.2021.126589.

[6] A. Patel, S.K. Patel, R.S. Singh, R.P. Patel, Review on recent advancements in the role of electrolytes and electrode materials on supercapacitor performances, Discover Nano 19 (2024). https://doi.org/10.1186/s11671-024-04053-1.

[7] W. Zhou, T. Huang, Y. Zhao, D. Kang, C. Huang, M. Ding, Ternary-metal Prussian blue analog hollow spheres/MXene electrode based on self-assembly enabling highly stable capacitive deionization, Chemical Engineering Journal 508 (2025) 161124. https://doi.org/10.1016/J.CEJ.2025.161124.

[8] R. Liu, Y. Wang, Y. Wu, X. Ye, W. Cai, Controllable synthesis of nickel–cobalt-doped Prussian blue analogs for capacitive desalination, Electrochimica Acta 442 (2023). https://doi.org/10.1016/J.ELECTACTA.2023.141815.

[9] Y. Ren, F. Yu, X.G. Li, B. Yuliarto, X. Xu, Y. Yamauchi, J. Ma, Soft-hard interface design in super-elastic conductive polymer hydrogel containing Prussian blue analogues to enable highly efficient electrochemical deionization, Materials Horizons 10 (2023) 3548–3558. https://doi.org/10.1039/D2MH01149B.

[10] X. Yang, H. Jiang, W. Zhang, T. Liu, J. Bai, F. Guo, Y. Yang, Z. Wang, J. Zhang, A novel “butter-sandwich” Ti3C2Tx/PANI/PPY electrode with enhanced adsorption capacity and recyclability toward asymmetric capacitive deionization, Separation and Purification Technology 276 (2021). https://doi.org/10.1016/j.seppur.2021.119379.

[11] B. Zhao, Y. Wang, Z. Wang, Y. Hu, J. Zhang, X. Bai, Rational design of Core-Shell heterostructured CoFe@NiFe Prussian blue analogues for efficient capacitive deionization, Chemical Engineering Journal 487 (2024). https://doi.org/10.1016/j.cej.2024.150437.

[12] Y. Guo, Z. Chen, D. Jiang, Y. Li, W. Zhang, K. Kozumi, Y. Kang, Y. Yamauchi, Y. Sugahara, Evolution of CuCoFe Prussian blue analogues with open nanoframe architectures for enhanced capacitive deionization, Chemical Engineering Journal 495 (2024). https://doi.org/10.1016/j.cej.2024.153714.

[13] Y. Cai, W. Zhang, J. Zhao, Y. Wang, Flexible structural construction of the ternary composite Ni,Co-Prussian blue analogue@MXene/polypyrrole for high-capacity capacitive deionization, Applied Surface Science 622 (2023). https://doi.org/10.1016/j.apsusc.2023.156926.

[14] Q. Li, Y. Zheng, D. Xiao, T. Or, R. Gao, Z. Li, M. Feng, L. Shui, G. Zhou, X. Wang, Z. Chen, Faradaic Electrodes Open a New Era for Capacitive Deionization, (2020). https://doi.org/10.1002/advs.202002213.

[15] L. Guo, D. Kong, M.E. Pam, S. Huang, M. Ding, Y. Shang, C. Gu, Y. Huang, H.Y. Yang, The efficient faradaic Li4Ti5O12@C electrode exceeds the membrane capacitive desalination performance, J Mater Chem A Mater 7 (2019) 8912–8921. https://doi.org/10.1039/C9TA00700H.

[16] C. Zhang, D. He, J. Ma, W. Tang, T.D. Waite, Faradaic reactions in capacitive deionization (CDI) - problems and possibilities: A review, Water Res 128 (2018) 314–330. https://doi.org/10.1016/j.watres.2017.10.024.

[17] M. Abraham, Preparation of And Application of Carbon Aerogel/Cobalt Phosphate Composite for Desalination by Hybrid Capacitive Deionization Method, International Journal of Chemistry and Chemical Processes E-ISSN 11 (n.d.) 2025. https://doi.org/10.56201/ijccp.vol.11.no2.2025.pg77.88.

[18] J. Cao, Y. Wang, L. Wang, F. Yu, J. Ma, Na(3)V(2)(PO(4))(3)@C as Faradaic Electrodes in Capacitive Deionization for High-Performance Desalination., Nano Lett 19 (2019) 823–828. https://doi.org/10.1021/acs.nanolett.8b04006.

[19] L. Ren, J.G. Wang, H. Liu, M. Shao, B. Wei, Metal-organic-framework-derived hollow polyhedrons of prussian blue analogues for high power grid-scale energy storage, Electrochim Acta 321 (2019). https://doi.org/10.1016/j.electacta.2019.134671.

[20] X. Guo, J. Zhang, J. Song, W. Wu, H. Liu, G. Wang, MXene encapsulated titanium oxide nanospheres for ultra-stable and fast sodium storage, Energy Storage Mater 14 (2018) 306–313. https://doi.org/10.1016/j.ensm.2018.05.010.

[21] Q. Liu, Z. Hu, M. Chen, C. Zou, H. Jin, S. Wang, S.L. Chou, Y. Liu, S.X. Dou, The Cathode Choice for Commercialization of Sodium-Ion Batteries: Layered Transition Metal Oxides versus Prussian Blue Analogs, Adv Funct Mater 30 (2020). https://doi.org/10.1002/ADFM.201909530.

[22] S. Vafakhah, L. Guo, D. Sriramulu, S. Huang, M. Saeedikhani, H.Y. Yang, Efficient Sodium-Ion Intercalation into the Freestanding Prussian Blue/Graphene Aerogel Anode in a Hybrid Capacitive Deionization System, ACS Appl Mater Interfaces 11 (2019) 5989–5998. https://doi.org/10.1021/ACSAMI.8B18746.

[23] X. Gao, Z. Fu, Y. Sun, D. Wang, X. Wang, Z. Hou, J. Wang, X. Liu, S. Wang, S. Yao, H. Zhang, S. Li, Z. Tang, W. Fu, K. Nie, J. Xie, Z. Yang, Y.M. Yan, Efficient hybrid capacitive deionization with MnO2/g-C3N4 heterostructure: Enhancing Mn dz2 electron occupancy by interfacial electron bridge for fast charge transfer, Desalination 567 (2023). https://doi.org/10.1016/j.desal.2023.116981.

[24] L. Hu, P. Jiang, P. Zhang, G. Bian, S. Sheng, M. Huang, Y. Bao, J. Xia, Amine-graphene oxide/waterborne polyurethane nanocomposites: effects of different amine modifiers on physical properties, J Mater Sci 51 (2016) 8296–8309. https://doi.org/10.1007/S10853-016-9993-5.

[25] P. Zhang, R.A. Soomro, Z. Guan, N. Sun, B. Xu, 3D carbon-coated MXene architectures with high and ultrafast lithium/sodium-ion storage, Energy Storage Mater 29 (2020) 163–171. https://doi.org/10.1016/J.ENSM.2020.04.016.

[26] G. Bharath, A. Hai, K. Rambabu, F. Ahmed, A.S. Haidyrah, N. Ahmad, S.W. Hasan, F. Banat, Hybrid capacitive deionization of NaCl and toxic heavy metal ions using faradic electrodes of silver nanospheres decorated pomegranate peel-derived activated carbon, Environ Res 197 (2021). https://doi.org/10.1016/J.ENVRES.2021.111110.

[27] K. Wei, Y. Zhang, W. Han, J. Li, X. Sun, J. Shen, L. Wang, A novel capacitive electrode based on TiO2-NTs array with carbon embedded for water deionization: Fabrication,

characterization and application study, Desalination 420 (2017) 70–78. https://doi.org/10.1016/J.DESAL.2017.07.001.

[28] A. Izadi-Najafabadi, S. Yasuda, K. Kobashi, T. Yamada, D.N. Futaba, H. Hatori, M. Yumura, S. Iijima, K. Hata, Extracting the full potential of single-walled carbon nanotubes as durable supercapacitor electrodes operable at 4 v with high power and energy density, Advanced Materials 22 (2010). https://doi.org/10.1002/adma.200904349.

[29] P. Díaz Baizán, Z. Arias, R. Santamaría, M. Ferreira, R. Menéndez, C. Blanco, Enhanced energy density of carbon-based supercapacitors using Cerium (III) sulphate as inorganic redox electrolyte, Electrochim Acta 168 (2015). https://doi.org/10.1016/j.electacta.2015.03.187.

[30] A.S. Yasin, H.O. Mohamed, I.M.A. Mohamed, H.M. Mousa, N.A.M. Barakat, Enhanced desalination performance of capacitive deionization using zirconium oxide nanoparticles-doped graphene oxide as a novel and effective electrode, Sep Purif Technol 171 (2016) 34–43. https://doi.org/10.1016/j.seppur.2016.07.014.

[31] K. Xu, X. Ji, C. Chen, H. Wan, L. Miao, J. Jiang, Electrochemical double layer near polar reduced graphene oxide electrode: Insights from molecular dynamic study, Electrochim Acta 166 (2015) 142–149. https://doi.org/10.1016/j.electacta.2015.03.101.

[32] A. Kalfa, T.R. Penki, I. Cohen, N. Shpigel, E. Avraham, D. Aurbach, D. Liang, Q. Wu, H. Wang, Y. Xiang, Thermally reduced graphene oxide as an electrode for CDI processes: A compromise between performance and scalability?, Desalination 492 (2020). https://doi.org/10.1016/j.desal.2020.114599.

[33] A.G. El-deen, J. Choi, C. Sang, K. Abdelrazek, A.A. Almajid, N.A.M. Barakat, TiO 2 nanorod-intercalated reduced graphene oxide as high performance electrode material for membrane capacitive deionization, 361 (2015) 53–64.

[34] S. Li, Y. Chen, X. He, X. Mao, Y. Zhou, J. Xu, Y. Yang, Modifying Reduced Graphene Oxide by Conducting Polymer Through a Hydrothermal Polymerization Method and its Application as Energy Storage Electrodes, (2019).

[35] J. Yu, Y. Liu, X. Zhang, R. Liu, Q. Yang, S. Hu, H. Song, P. Li, A. Li, S. Zhang, Enhanced capacitive deionization of a low-concentration brackish water with protonated carbon nitride-decorated graphene oxide electrode, Chemosphere 293 (2022). https://doi.org/10.1016/j.chemosphere.2022.133580.

[36] J. Cui, T. Huang, Y. Zhao, A. Bentley, M. Xu, L. Guo, M. Ding, H.Y. Yang, Unveiling the sodium adsorption behavior of controlled NaTi2(PO4)3 on Ti3C2Tx MXene for balanced salt adsorption capacity and cycling stability, Sep Purif Technol 339 (2024). https://doi.org/10.1016/j.seppur.2024.126613.

[37] C. Zhang, D. He, J. Ma, W. Tang, T.D. Waite, Faradaic reactions in capacitive deionization (CDI) - problems and possibilities: A review, Water Res 128 (2018) 314–330. https://doi.org/10.1016/j.watres.2017.10.024.

[38] J.H. Choi, Determination of the electrode potential causing Faradaic reactions in membrane capacitive deionization, Desalination 347 (2014) 224–229. https://doi.org/10.1016/j.desal.2014.06.004.